

Effects of charge-orbital order-disorder phenomena on the unoccupied electronic states in the single-layered half-doped $\text{Pr}_{0.5}\text{Ca}_{1.5}\text{MnO}_4$

V. Capogrosso,¹ M. Malvestuto,^{2,3,*} I. P. Handayani,⁴ P. H. M. van Loosdrecht,⁴ A. A. Nugroho,⁵ E. Magnano,³ and F. Parmigiani^{1,2}

¹*Department of Physics, University of Trieste, via A. Valerio 2, I-34127 Trieste, Italy*

²*Elettra-Sincrotrone Trieste, Area Science Park-Basovizza, S. S. 14, Km.163.5, I-34149 Trieste, Italy*

³*IOM-CNR, Laboratorio TASC, Area Science Park-Basovizza, S. S. 14, Km.163.5, I-34149 Trieste, Italy*

⁴*Zernike Institute for Advanced Materials, University of Groningen, Nijenborgh 4, NL-9747 AG Groningen, The Netherlands*

⁵*Faculty of Mathematics and Natural Sciences, Institute of Technology Bandung, Jl. Ganesha 10 Bandung, 40132 Indonesia*

(Received 7 November 2012; published 10 April 2013)

Here we report a study on the unoccupied states of the half-doped $\text{Pr}_{0.5}\text{Ca}_{1.5}\text{MnO}_4$ (PCMO). Our investigation, based on temperature dependent x-ray absorption linear dichroism (XLD) and density-functional theory discloses the role of the charge-orbital ordering-disordering mechanisms on the unoccupied density of states. In particular, the lowest unoccupied band has a Mn e_g $d_{3z^2-r^2}$ character, proving that the physical properties of the two-dimensional (2D) PCMO are also determined by the out-of-plane orbital. Yet, the difference in energy between the $d_{3z^2-r^2}$ and $d_{x^2-y^2}$ states is observed to increase when a charge-orbital ordering is established, hence revealing that the Mn 3d electronic hopping is frustrated when the MnO_6 cluster orthorhombic strain is increased. This finding addresses the question concerning the complex interplay between the in-plane and out-of plane orbitals in these 2D half-doped single layered manganites.

DOI: [10.1103/PhysRevB.87.155118](https://doi.org/10.1103/PhysRevB.87.155118)

PACS number(s): 71.15.Ap, 71.27.+a, 71.30.+h, 78.70.Dm

I. INTRODUCTION

Understanding the orbital physics of the rare earth manganites of the Ruddlesden-Popper single layered structure, having the general composition $R_{1-x}A_x\text{MnO}_4$ (R is rare earth; A is alkaline earth), is a complex and challenging question for its intimate correlation with the general problem of charge and magnetic ordering.^{1,2} In many layered or pseudocubic manganite systems, orbital ordering is found to be at the origin of the anisotropy of the electron-transfer interaction, which may favor or disfavor the double-exchange interaction or superexchange interaction that depends on the orbital direction determined by a complex spin-orbital coupled state.

The mechanism that drives the ordering phenomena leading to these orbital effects is still a matter of significant disagreement, although the orbital lattice coupling and the electron hopping (along with on-site Coulomb interaction) are generally believed to be the main mechanisms to be considered.²

In this context, the single layered half-doped $\text{Pr}_{0.5}\text{Ca}_{1.5}\text{MnO}_4$ (PCMO) is a case study for layered systems displaying charge, orbital, and magnetic orderings. Interestingly though, PCMO also displays a peculiar low temperature (orbitally induced) spin-lattice coupling³ that is missing in other rare-earth doped layered manganites. Furthermore, PCMO exhibits a charge-orbital ordering (CO-O) transition at a remarkably high T_{CO} ,⁴ slightly above room temperature, accompanied by an orthorhombic structural distortion,⁵ where the strongly correlated Mn e_g charge carriers order onto separate crystallographic sublattices (charge ordered state) with a specific orbital character (symmetry) (orbital ordered state).

In layered manganite systems, the unoccupied density of states (DOS), orbital degeneracy, and orbital polarization are information that can be obtained by x-ray polarization depen-

dent absorption spectroscopies, by tuning the x-ray energy at Mn and O edges. The x-ray absorption linear dichroisms (XLDs) at the O K and Mn $L_{2,3}$ edges have been extensively studied⁶⁻¹³ to assess the topology of the orbital states close to the Fermi energy where the O $2p$ orbitals, σ bonded to the Mn $3d_{3z^2-r^2}$ and $3d_{x^2-y^2}$ orbitals, are dominant.¹⁴⁻¹⁶ While the Mn L_{23} XLD has been widely exploited to investigate the orbital and magnetic orderings, similar studies at the O K edge are less common. The advantage of studying the O K -edge XLD in anisotropic manganites results from the fact that this spectroscopy allows one to separate the contributions to the unoccupied DOS⁶⁻⁹ of the in-plane and the out-of-plane oxygen sites.

While a number of oxygen and manganese XLD studies have been reported on layered manganites across the antiferromagnetic (AFM) transitions, experimental data across the CO-O transition are very limited. In general, a clear knowledge about the role of the oxygen $2p$ states on the unoccupied electronic states is lacking, while a complete study of the PCMO unoccupied electronic states is still missing.

To elucidate the role of the O $2p$ orbital topology in the rearrangement of the unoccupied O $2p$ - Mn $3d$ DOS across the ordered-disordered phases of the PCMO, we investigate the temperature dependent XLD¹⁷⁻¹⁹ at the O K threshold. The reported investigation assesses the nature of the unoccupied DOS by means of a detailed study supported by *ab-initio* calculations of the O K threshold and the relative XLD signal measured at three distinct phases of the PCMO.³ The analysis of the linear dichroic (LD) at the O K edge allows one to map and disentangle the partial density of empty O $2p$ states at the oxygen site and the local symmetry of the Mn empty states at once, since the O $2p$ states are hybridized with the metal states.²⁰ The oxygen data are completed and corroborated by the XLD data taken at the Mn $L_{2,3}$. The spectra are qualitatively discussed and compared with experimental and calculated

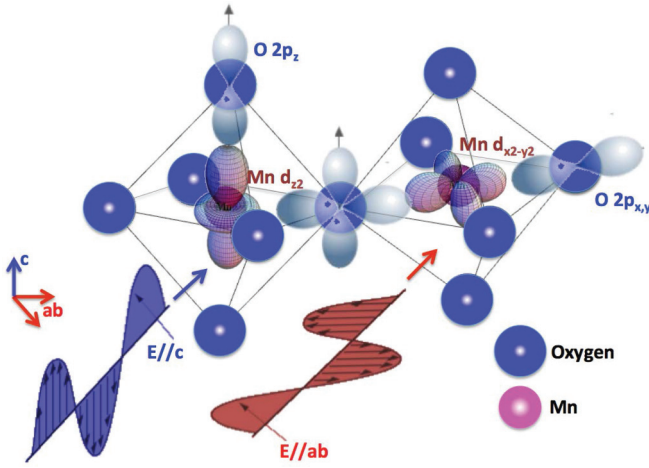


FIG. 1. (Color online) Scheme of the light electric field components with respect to the orientation of the Mn e_g and O $2p$ orbitals in the Mn-O octahedra of the PCMO single crystal. The vertical light ($E \parallel c$) polarization (blue) probes the out-of-plane states and the horizontal ($E \parallel ab$) one (red) probes the in-plane states.

data found in the literature in order to assess the orbital and magnetic state of the sample.

Finally, we report important information about the intralayer redistribution of the ligand holes, that is associated to an increasing of the energy difference between the $d_{3z^2-r^2}$ and $d_{x^2-y^2}$ orbitals and to a dramatic change of the Mn $L_{2,3}$ linear dichroic signal below T_{CO} . We interpret the former two effects as the out-of-plane charge carriers localization resulting from the competing orbital-lattice coupling and the electron hopping charge dynamics, being the latter a signature of the onset of the e_g orbital order.

II. METHODS

A. Experimental section

This work was carried out on beamline BACH^{21,22} at the Elettra radiation synchrotron facility. Single crystal PCMO was grown using a floating zone technique.²³ For the experiments, crystal platelets of the desired orientation were cut from a single grown rod. The lattice structure and high sample quality was confirmed by x-ray diffraction experiments. The sample was mounted with the *c* axis of the crystal perpendicular to the beam direction as sketched in Fig. 1. The scattering angle was set at 0° in order to avoid spurious matrix element and geometrical effects. The sample temperature during the experiment was monitored by a thermocouple attached to the sample. The crystal was broken in an UHV condition (5×10^{-10} mbar) and the presence of surface contaminants was checked measuring the C $1s$ spectra by x-ray photoemission. The end station is fitted with a variable temperature sample holder for total electron yield (TEY) measurements. The X-ray Absorption Spectroscopy (XAS) spectra were taken at the Mn $2p$ and O $1s$ edges varying the x-ray beam linear polarization in order to measure XAS linear dichroism, from $E \parallel c$ (vertical polarization) to $E \parallel ab$ (horizontal polarization) (Fig. 1). The XAS spectra were measured in TEY mode in order to minimize the strong self-absorption effects present at the Mn L_3 edge. Finally, XAS spectra were normalized to the beam flux and

aligned on the photon energy scale using Fermi edges recorded from an Au foil.

B. Computer modeling

The XAS data have been interpreted on the base of an *ab-initio* Local Density Approximation model, applicable to the crystal structure at room-temperature. The electronic structure calculations have been carried out using the linearized augmented plane wave (LAPW) method within density-functional theory (DFT), as implemented in the WIEN2K code.²⁷ The crystal structure at room temperature is orthorhombic with space group $Pnma$ and lattice constants $a = 5.4071(3)$ Å, $b = 5.3409(7)$ Å, and $c = 11.7018(11)$ Å.²⁸ The *muffin-tin* sphere radii were set to 2.08, 1.85, and 1.64 bohrs for Ca (Pr), Mn, and O atoms, respectively. To determine the basis size, R_{MT} = Muffin Tin Radius; K_{max} = magnitude of the largest K vector (=reciprocal lattice vector) was fixed at 5.0. We set 100 k points for integration over the Brillouin zone, which ensure a sufficient accuracy of the results. The exchange and correlation effects were treated by using the local spin density approximation plus Hubbard repulsion (U) (LSDA + U). In order to simulate the strongly correlated nature of the $3d$ electrons, an *on-site* Coulomb contribution ($U = 0.6$ Ry) was added to simulate the strongly correlated nature of the $3d$ electrons. The resulting partial Mn $3d$ and O $2p$ DOS are reported in Fig. 3.

III. RESULTS AND DISCUSSION

The polarization dependent O K XAS spectra taken at three different temperatures [above the CO-O transition ($T_{340K} > T_{CO(=320K)}$), below T_{CO} ($T_N < T_{300K} < T_{CO(=320K)}$), and below the AFM transition ($T_{100K} < T_{N(=120K)}$)] are shown in Figs. 2(b)–2(d), respectively. The corresponding LD spectra, defined as the difference between the out-of-plane and the in-plane polarizations, i.e., $LD = XAS_{E \parallel c} - XAS_{E \parallel ab}$, are also reported. In addition, we calculated $\Delta\mu_{XAS}(T) = \mu_{XAS}(T) - \mu_{XAS}(340\text{ K})$ [Fig. 2(e)] which directly represents the spectral variations versus temperature.

The O K XAS is associated with the O $1s \rightarrow 2p$ dipole transition, whose absorption intensity is

$$W_{i \rightarrow f} = \frac{2\pi}{\hbar} |\langle i | H' | f \rangle|^2 g(\hbar\omega),$$

where

$$H' = e\hat{\epsilon} \cdot r \text{ (dipole approximation).}$$

In the O^{2-} ion, the $2p$ orbital is full but strong hybridization with the unoccupied Mn $3d$ states induces O $2p$ holes. Thus, the strength of the O $1s \rightarrow 2p$ transition reflects the unoccupied conduction band consisting of states with a Mn $3d$ character. In fact, in a configuration interaction approach to the general problem of the MnO_6 atomic cluster,^{16,29} the ground state is a linear combination of $3d$ and $3d\bar{L}$ electron configurations, where \bar{L} denotes a ligand hole (O $2p$ hole). More specifically, considering the orbital symmetries of the e_g orbitals, the electronic ground states of the Mn sites result in a superposition of two distinct electronic configurations:

$$\begin{aligned} & \alpha \cdot 3d^4 + \beta \cdot 3d^5_{(x^2-y^2)} \bar{L}_{(x^2-y^2)}, \\ & \gamma \cdot 3d^3 + \delta \cdot 3d^4_{(3z^2-r^2)} \bar{L}_{(3z^2-r^2)}, \end{aligned}$$

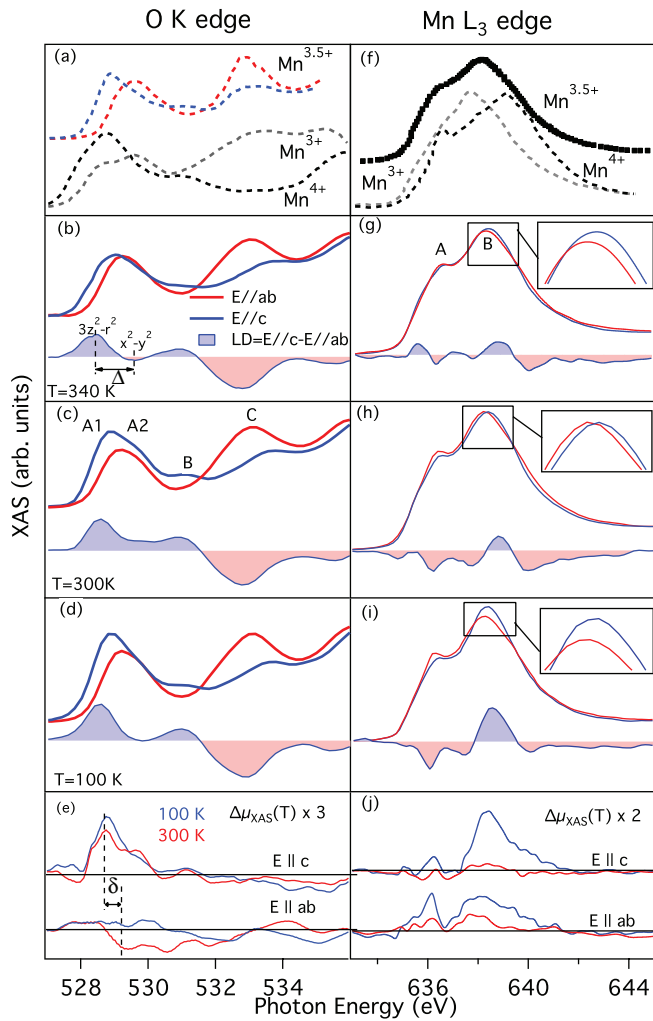


FIG. 2. (Color online) Polarization dependent O K (on the left) and Mn L_3 (on the right) X-ray Absorption Near Edge Spectroscopy spectra of $\text{Pr}_{0.5}\text{Ca}_{1.5}\text{MnO}_4$, measured with the electric field E along the ab axis (red curve) and along the c axis (blue curve), taken at three different temperatures corresponding to the charge-orbital disordered [(b) and (g)], ordered [(c) and (h)], and AFM [(d) and (i)] states. For each pair of spectra the XAS linear dichroism ($\text{LD} = \text{XAS}_{E\parallel c} - \text{XAS}_{E\parallel ab}$) is reported. The top panels show (a) O K and (f) Mn L_3 XAS spectra of different reference compounds: (a) LSMO (Ref. 6) measured with $E \parallel ab$ (dotted red curve), $E \parallel c$ (dotted blue curve), CaMnO_3 (Ref. 24) (dotted black curve), and LaMnO_3 (Ref. 24) (dotted gray curve); (f) MnO_2 (Ref. 25) (dotted black curve), LaMnO_3 (Ref. 25) (dotted gray curve), and $\text{La}_{0.5}\text{Sr}_{1.5}\text{MnO}_4$ (Ref. 26) (heavy black curve). The bottom panels [(e) and (j)] show the corresponding spectral variations, $\Delta\mu_{\text{XAS}}(T) = \mu_{\text{XAS}}(T) - \mu_{\text{XAS}}(340 \text{ K})$, as a function of temperature (see text).

where $\underline{L}_{(x^2-y^2)}$ and $\underline{L}_{(3z^2-r^2)}$ denote O $2p$ holes induced by the hybridization with $3d_{3z^2-r^2}$ and $3d_{x^2-y^2}$ orbitals, respectively. Accordingly, as illustrated in Fig. 1, the O $2p$ holes with $x^2 - y^2$ and $3z^2 - r^2$ characters belong to the in-plane and out-of-plane O ions, respectively. Therefore, due to the selection rules dictated by the transition matrix element H' in the dipole approximation,³⁰ the absorption strength for the $E \parallel c$ and $E \parallel ab$ incoming photon polarizations reflects the symmetry of the unoccupied Mn $3d$ orbitals and selectively probes the Mn- O_a

(apical) and Mn- O_p (planar) bonds, respectively, allowing one to probe the three-dimensional (3D) oxygen orbital topology.

The O K XAS spectra of PCMO display four prominent features in the 527.5–536 eV range, which are marked as A_1 , A_2 , B , and C [see Fig. 2(c)] showing a notable dichroism between the electric field parallel to the c axis and the ab plane. The line shape of the O K edge is similar to the O K edge measured in other layered manganites—and other perovskites as well. In particular, the first 5 to 8 eV above the absorption edge are characterized by the strong hybridization between O $2p$ and Mn $3d$ orbitals.^{10,16,31,32} For PCMO the first spectral energy region, between 527.5 and 530.5 eV, shows a double-peak feature (A_1 and A_2) in the $E \parallel c$ polarization geometry, whereas only a single-peak feature (A_2) is detected in $E \parallel ab$ geometry.^{6,14}

A comparison between the PCMO spectra and their equivalent measured on the half-doped $\text{La}_{0.5}\text{Sr}_{1.5}\text{MnO}_4$ (LSMO) [Fig. 2(a)] allows one to assign the feature A_1 to the Mn $3d_{z^2}$ - O_a $2p_z$ bonding, whereas the feature A_2 is ascribed to the planar O_p $2p_x$ and O $2p_y$ orbitals hybridized with Mn $d_{x^2-y^2}$ states. These states are energetically close to the spatially isotropic Mn t_{2g} -down states.^{6,11,14,33} Because of the different orbital geometry and the difference in the absorption energy (Δ) for the in-plane and out-of-plane $3d$ orbitals, the measured LD XAS signals exhibit features that support the above assignments. The calculations corroborate the observed linear dichroism by revealing that the Mn e_g up and down states and the t_{2g} states extend for 7 eV. The apical O p_z are found to strongly overlap with the Mn $d_{3z^2-r^2}$ (up and down) and the $3d_{x_z, y_z}$ down states. Ergo, the different DOS distributions of the O p_z (parallel to the c axis) and O p_{xy} DOS (parallel to the ab plane) explain the dichroic effect observed in the O K XAS spectra.

The feature B is commonly ascribed to either t_{2g} -down states or to an upper Hubbard band.^{6,7} A direct comparison between the measured XAS spectra on PCMO and those taken on Mn^{4+} (CaMnO_3)²⁴ and Mn^{3+} (LaMnO_3)²⁴ can help to clarify this assignment. For $E \parallel c$, the PCMO XAS spectrum mirrors that of the Mn^{4+} (strong A_1 , B present), while for $E \parallel ab$ it resembles that of Mn^{3+} (A_1 strongly depleted, A_2 present, B absent). Correspondingly, the B feature can be attributed to the direct hybridization of Mn $3d_{z^2}$ - O_a $2p_z$ and $3d_{x_z, y_z}$ - O_p $2p_x$. That is confirmed by the calculated oxygen DOS for the apical and basal oxygens as shown in Fig. 3. Finally, the observed affinity reflects the electronic anisotropy in this electronic ground states for the Mn ions. In fact, we observe a Mn^{4+} -like character along the c axis and a Mn^{3+} -like character in the ab basal plane. This anisotropy reflects the almost complete localization of the e_g charge carriers in the low energy out-of-plane orbitally polarized states, as expected for a layered structure.

The tendency of the charge carriers to localize in the lowest unoccupied energy state can be frustrated by the electron hopping mechanism. This mechanism, as discussed in the following, tends to delocalize the charges in the basal plane.

The energy difference $\Delta E = \epsilon(d_{3z^2-r^2}) - \epsilon(d_{x^2-y^2})$ versus temperature (see Table I) has a ground state depending on two competing mechanisms. The local MnO_6 distortion removes the Mn $3d$ orbital degeneracy forcing the charge carriers in the out-of-plane $3d_{z^2}$ orbital and the charge dynamics of electron hopping tends to delocalize the charges in the basal plane.

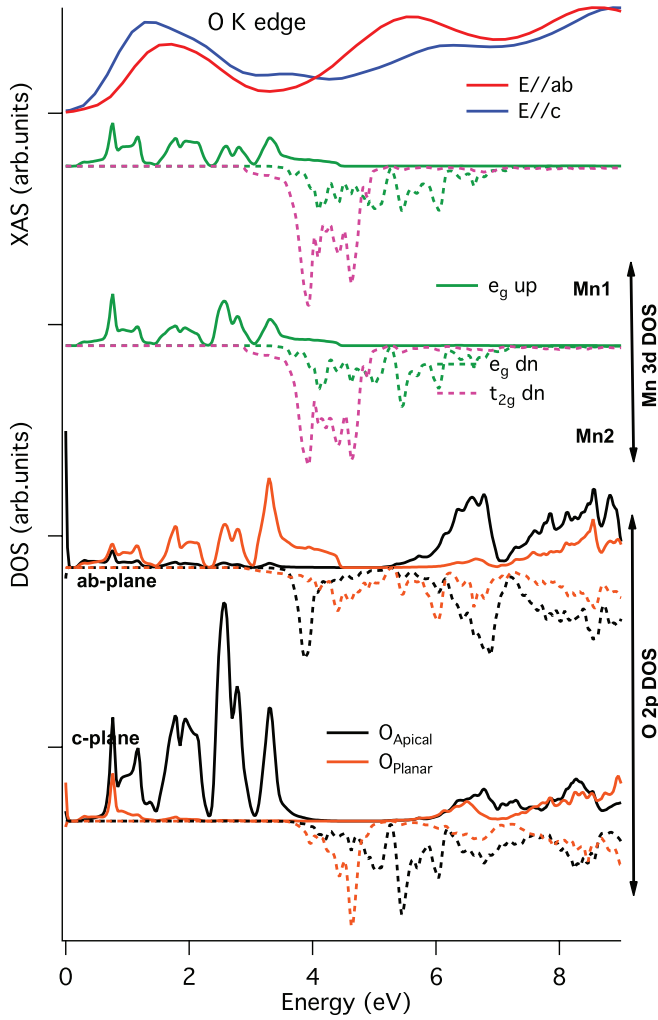


FIG. 3. (Color online) Comparison of the experimental O *K* XAS spectra for $E \parallel ab$ (red curve) and $E \parallel c$ (blue curve), measured at $T = 300$ K, to the calculated O *2p* and Mn *3d* DOS. The Mn *3d* DOS-up (solid line) and -down (dotted line) are singled out between the two atomic sites Mn₁ and Mn₂ and resolved with respect to the e_g (green curve) and t_{2g} (pink curve) symmetries. The O DOS-up and -down are projected along the *a*, *b*, and *c* directions and singled out between planar (orange curve) and apical (black curve) oxygen sites.

Considering the core-hole binding energy difference [δ , see Fig. 2(e)] at the apical and basal oxygen sites due to the different coordination, it is also possible to estimate the orbital energy difference $\Delta E = \Delta - \delta$.

In order to study how the charge-orbital order-disorder phenomena affect ΔE , the O *K* XAS spectra, along with

TABLE I. The experimental energy difference $\Delta E = \epsilon(d_{3z^2-r^2}) - \epsilon(d_{x^2-y^2})$, $\Delta = \Delta E + \delta$ [see Fig. 2(b)], and the core-hole energy difference δ [see Fig. 2(e)] at the in- and out-of-plane oxygen sites.

T (K)	ΔE (eV)	Δ (eV)	δ (eV)
100	0.58	1.21	0.63
300	0.57	1.2	0.63
350	0.46	1.09	0.63

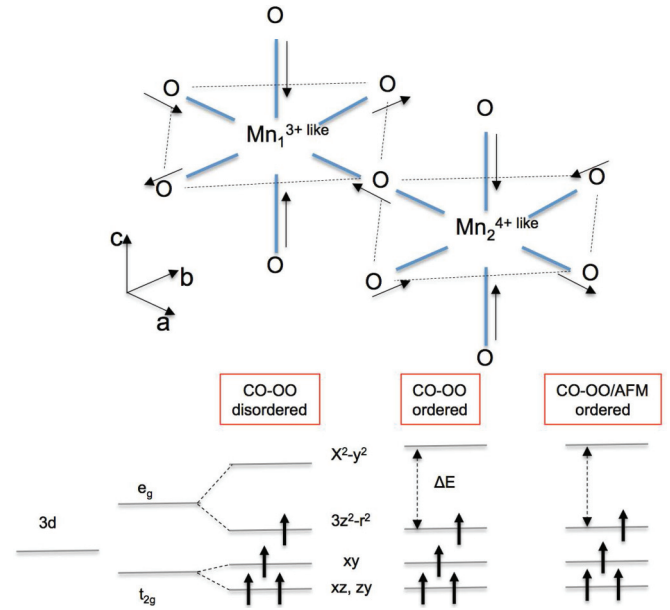


FIG. 4. (Color online) (Top) Sketch of the orthorhombic distortion of the adjacent Mn³⁺-like and Mn⁴⁺-like MO₆ octahedra. (Bottom) Schematic energy diagram of the Mn *3d* electronic states in the CO disordered and ordered phases.

the related XLDs, and $\Delta\mu_{\text{XAS}}(T)$ signals versus T must be considered. For each polarization the XAS edges are conserved, beside some irrelevant variation of the main features intensity. In the charge-orbital disordered phase ($T = 340$ K), the intensities of A_1 and A_2 are identical, whereas the intensity of B is less pronounced with respect to the low temperature cases. When the system undergoes the CO-O transition, its unit cell shows a strong enhancement of the orthorhombic strain in the basal Mn-O plane for allowing the orbital ordering to be established.³

The orthorhombicity of the MnO₆ octahedra reflects a change of the conduction band DOS, characterized by the appearance of a double-peak feature which now appears as a distinct double-peak feature in the $E \parallel c$ XAS spectra [Fig. 2(e)]. Consistently, $\Delta\mu_{\text{XAS}}(T = 300$ K), for $E \parallel ab$, is positive and double peaked (A_1 and A_2), proving an increased DOS for the out-of-plane states. Interestingly, the corresponding variation of $\Delta\mu_{\text{XAS}}(T = 300$ K) for $E \parallel ab$ is negative.

Therefore, the associated decreasing of the Mn- O_a distance (see top panel of Fig. 4) and the increasing difference of the basal Mn- O_p distances in the CO-O phase, result in an injection of holes in the out-of-plane states and a reduction of the in-plane oxygen *2p* DOS, i.e., in a charge transfer from out-of-plane to in-plane states. This mechanism seems to be in contrast with the increasing value of ΔE [from 0.46 eV (disordered phase) to 0.57 eV (ordered phase)]. Indeed, this process would favor the transfer of charge carriers in the out-of-plane electronic states. This apparent disagreement can be overtaken by considering the binding energies of the Mn e_g ground state resulting from the Coulomb term of the crystal field (CF) and the kinetic term of electron hopping (eh):

$$\Delta E = (-CF(d_a) + eh(d_a))_{3z^2-r^2} - (-CF(d_p) + eh(d_p))_{x^2-y^2}, \quad (1)$$

where d_a and d_p are the Mn-O_a and Mn-O_p distances, respectively. Since the reduced out-of-plane/in-plane orthorhombicity tends to reduce the CF term, the competing out-of-plane/in-plane p - d hybridizations results in a larger ΔE . Furthermore, the decreased in-plane hopping integral can explain the increased resistivity below T_{CO} .³⁴

Interestingly, in the 528–531 eV energy range the intensity of $\Delta\mu_{XAS}(T = 100 \text{ K})$ for $E \parallel c$ increases further upon cooling, whereas the A_1/A_2 intensity ratio increases for the lower energy state. This observation can be ascribed to the additional decrease of the Mn-O_a distance resulting in a rise of the out-of-plane DOS. Conversely, the corresponding variation of $\Delta\mu_{XAS}(T = 100 \text{ K})$ for $E \parallel ab$ is positive. This finding is consistent with the reduced in-plane orthorhombic distortion. Therefore, the distinct behavior of the spectral variations $\Delta\mu_{XAS}(T)$ at $T = 300$ and 100 K can be explained by considering the reduced orthorhombicity taking place slightly above T_N .

Notably, the energy difference ΔE (see Table I, $T = 100$ and 300 K) remains equal to the value above T_N . This proves that the $3d e_g$ splitting and the charge dynamics electron hopping are not affected by the AFM ordering.

The oxygen data are completed and corroborated by the XLDs data taken at the Mn $L_{2,3}$. The XLD at the Mn $L_{2,3}$ are qualitatively discussed and compared with experimental and calculated data found in the literature in order to assess the orbital and magnetic states of the PCMO sample. Figure 2 shows the polarization dependent Mn $2p$ XAS spectra as measured for the CO-O disordered [at $T_{=340K} > T_{CO}$, Fig. 2(g)], ordered [$T_N < T_{=300K} < T_{CO}$, Fig. 2(h)], and the CO-O antiferromagnetic [$T_{=100K} < T_N$, Fig. 2(i)] phases. The Mn L_3 linear dichroic signals and the spectral variations $\Delta\mu_{XAS}(T)$ [Fig. 2(j)] are also reported.

The Mn L_3 thresholds are compared [see Fig. 2(f)] to the corresponding spectra of the formally tetravalent Mn⁴⁺ [MnO₂ (Ref. 25)], trivalent Mn³⁺ [LaMnO₃ (Ref. 25)], and half-doped Mn^{3.5+} [LSMO (Ref. 9)]. This qualitative comparison confirms the $3d^{3.5}$ configuration of the Mn ions in PCMO and the admixture of Mn⁴⁺-like and Mn³⁺-like sites, regardless of the temperature.

The main spectral features (A and B) stem from excitations of core electrons from the $2p$ manifold to unoccupied $3d$ states, i.e., transitions from $2p^6 3d^n$ ground states to different excited multiplet configurations. Accordingly with *ab-initio* calculations on similar layered manganites,^{10,35,36} the Mn L_3 line shape is determined by the coexistence of Mn⁴⁺-like and Mn³⁺-like ions, while the structure A reflects the presence of Mn⁴⁺-like sites.

The intensity and the energy positions of these features and of the overall $L_{2,3}$ line shape exhibit a significant linear dichroism upon the change of polarization. Considering the disordered state ($T > T_{CO}$), the observed dichroism reflects the electronic ground state anisotropy induced by the local orthorhombic strain of the MnO₆ octahedra. This distortion significantly affects the LD signal, clearly proved by the direct comparison between the XLDs reported in Figs. 5(a) and 5(d), where the LD for PCMO at $T > T_{CO}$ and the calculated LSMO data,³⁸ respectively, are compared. The results shown in Fig. 5(d) derive from a many body cluster calculation for a tetragonally distorted MnO₆ cluster with a $\delta =$

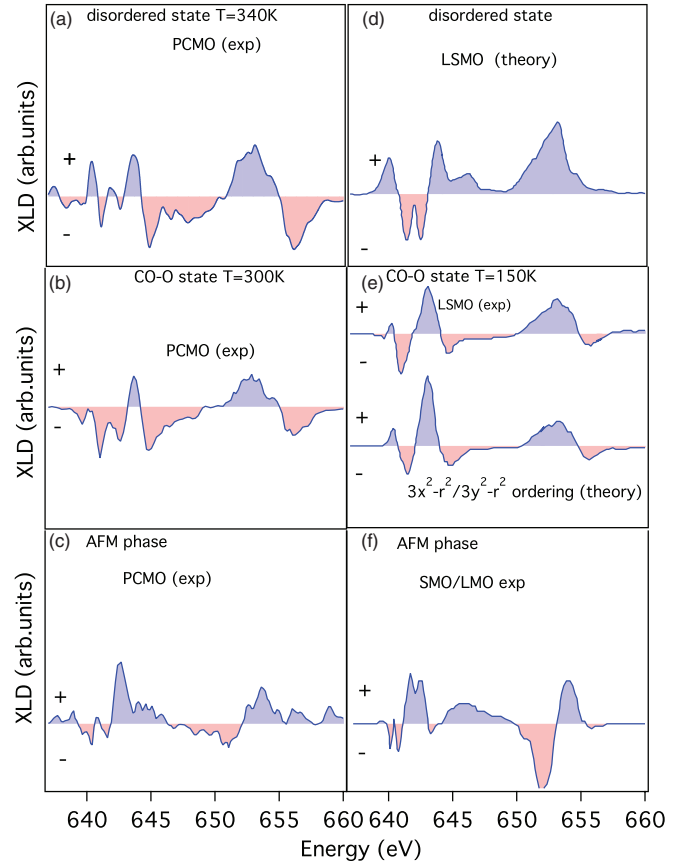


FIG. 5. (Color online) (a) Mn L_3 linear dichroism (LD = $XAS_{E\parallel c} - XAS_{E\parallel ab}$) signal measured at $T = 340 \text{ K}$ for PCMO; (b) LD signal at the Mn $L_{2,3}$ edge measured at $T = 300 \text{ K}$ for PCMO; (c) LD signal at the Mn $L_{2,3}$ edge for PCMO obtained by the difference between LD at 100 K and LD at 300 K ; (d) LD signal calculated for LSMO (Ref. 38); (e) LD signal at $T = 150 \text{ K}$ for LSMO (Ref. 26) and theoretically calculated for orbital scenarios with Mn³⁺ $3x^2 - r^2/3y^2 - r^2$ orbital occupation (Ref. 26); (f) AFM signal for SrMnO₃/LaMnO₃ films (Ref. 37).

0.05 , δ being the difference between apical and basal Mn-O distances.

When T is brought below T_{CO} , the Mn $L_{2,3}$ LD signal displays dramatic variations with respect to the disordered phase, as shown in Fig. 5. The LD line shape exhibits a pronounced negative-positive double-peaked contour in the L_3 region with the primary peaks corresponding to the A and B features of $L_{2,3}$. The LD signal for PCMO at $T = 300 \text{ K}$ [Fig. 5 (b)] can be compared to the measured LD signal for LSMO at $T = 150 \text{ K}$ where this compound is orbitally ordered [top spectrum of Fig. 5(e)].²⁶ The two LD signals are very similar and both are in agreement with the theoretically calculated Mn³⁺ $3x^2 - r^2/3y^2 - r^2$ (*rod-like*) orbital occupation [bottom spectrum of Fig. 5(e)].²⁶ These LD spectra have been simulated using the well-established configuration interaction cluster model including the full atomic multiplet theory. However, it must be considered that the LD signal is a linear combination of both a structural and an orbital ordering contributions. Hence, this argument has only a qualitative relevance.

Finally, the positive variation of $\Delta\mu_{\text{XAS}}(T = 300 \text{ K})$ along the *ab* plane is conveyed by a change of the relative intensities of peaks *A* and *B*. For the intensity of peak *A* is related to the relative concentration of Mn⁴⁺-like sites,^{10,15,39} the above mentioned variation can be attributed to a disproportionation of the different Mn sites induced by the charge ordering.

When *T* is below T_N , in the AFM phase, the overall line shape of the LD signal remains nearly identical to those detected for higher *T*, except for the dramatic intensity increase of the LD main spectral features. It is worth noting that the LD signal below T_N is now a linear combination of different contributions originating from the orthorhombic distortion, the orbital ordering, and the AFM induced anisotropy. Since the orbital ordering contribution to the LD signal should remain constant versus temperature, the intensity increase of $\Delta\mu_{\text{XAS}}(T = 100 \text{ K})$ is originated by the AFM contribution. The AFM contribution shown in Fig. 5(c) has been obtained by taking the difference between the LD at 100 K and LD at 300 K, and is compared to the AFM signal measured by Aruta *et al.*³⁷ on the SMO/LMO films [see Fig. 5(f)].

IV. CONCLUDING REMARKS

In conclusion, by taking advantage of the element specific temperature dependent linear dichroism of the O *K* x-ray

absorption edge, we have studied the effects of CO-O ordering on the low energy unoccupied states of the half-doped PCMO. The close inspection of the XLD and of the $\Delta\mu_{\text{XAS}}(T)$ signals uncovered crucial clues on the effects of CO-O ordering on the low energy unoccupied states resulting from the strong anisotropy of the Mn 3*d* - O 2*p* hybridized states. The present results show that the competitive interplay between the local atomic distortion, necessary for accommodating the CO-ordering and the charge dynamics of the hopping mechanism, regulates the orbital state of the charge carriers. In fact, while the diminished local distortion reduces the tendency of the charge carriers to localize in the lowest energy out-of-plane state, the different in-plane and out-of-plane *d-p* hybridization frustrates the $d_{3z^2-r^2} \leftrightarrow d_{x^2-y^2}$ hopping, disfavoring the in-plane charge transfer interaction between adjacent Mn sites.

ACKNOWLEDGMENTS

The authors are grateful to F. Cilento, M. Cuoco, D. Fausti, F. Forte, F. Novelli, and A. Verna for useful discussions. M.M. is grateful to Federico Salvador for technical support. F.P. acknowledges partial financial support by the MIUR-PRIN 2008 project.

*marco.malvestuto@elettra.trieste.it

¹M. Imada, A. Fujimori, and Y. Tokura, *Rev. Mod. Phys.* **70**, 1039 (1998).

²Y. Tokura, *Science* **288**, 462 (2000).

³S. Chi, F. Ye, P. Dai, J. A. Fernandez-Baca, Q. Huang, J. W. Lynn, E. W. Plummer, R. Mathieu, Y. Kaneko, and Y. Tokura, *Proc. Natl. Acad. Sci. USA* **104**, 10796 (2007).

⁴M. Ibarra, R. Retoux, M. Hervieu, C. Autret, A. Maignan, C. Martin, and B. Raveau, *J. Solid State Chem.* **170**, 361 (2003).

⁵K. S. Chao, D. J. Huang, J. Okamoto, H.-J. Lin, C.-H. Hsu, Y. Kaneko, R. Mathieu, W. B. Wu, Y. Tokura, and C. T. Chen, *J. Magn. Magn. Mater.* **310**, 819 (2007).

⁶M. Merz, P. Reutler, B. Büchner, D. Arena, J. Dvorak, Y. U. Idzerda, S. Tokumitsu, and S. Schuppler, *Eur. Phys. J. B* **51**, 315 (2006).

⁷M. Merz, G. Roth, P. Reutler, B. Büchner, D. Arena, J. Dvorak, Y. U. Idzerda, S. Tokumitsu, and S. Schuppler, *Phys. Rev. B* **74**, 184414 (2006).

⁸W. B. Wu, D. J. Huang, G. Y. Guo, H.-J. Lin, T. Y. Hou, C. F. Chang, C. T. Chen, A. Fujimori, T. Kimura, H. B. Huang, A. Tanaka, and T. Jo, *J. Electron Spectrosc. Relat. Phenom.* **137-140**, 641 (2004).

⁹D. J. Huang, W. B. Wu, G. Y. Guo, H.-J. Lin, T. Y. Hou, C. F. Chang, C. T. Chen, A. Fujimori, T. Kimura, H. B. Huang, A. Tanaka, and T. Jo, *Phys. Rev. Lett.* **92**, 087202 (2004).

¹⁰M. Platié, F. Bondino, M. Zacchigna, M. Zangrando, I. Alessandri, M. Affronte, L. Malavasi, and F. Parmigiani, *Phys. Rev. B* **72**, 085102 (2005).

¹¹J. Herrero-Martin, J. Garcia, G. Subias, J. Blasco, and M. C. Sánchez, *Phys. Rev. B* **72**, 085106 (2005).

¹²G. Subías, J. García, M. Sánchez, J. Blasco, and M. Proietti, *Surf. Rev. Lett.* **9**, 1071 (2002).

¹³K. Kuepper, F. Bondino, K. C. Prince, M. Zangrando, M. Zacchigna, A. F. Takács, T. Crainic, M. Matteucci, F. Parmigiani, A. Winiarski, V. R. Galakhov, Y. M. Mukovskii, and M. Neumann, *J. Phys. Chem. B* **109**, 15667 (2005).

¹⁴J.-H. Park, T. Kimura, and Y. Tokura, *Phys. Rev. B* **58**, R13330 (1998).

¹⁵F. M. F. de Groot, J. C. Fuggle, B. T. Thole, and G. A. Sawatzky, *Phys. Rev. B* **42**, 5459 (1990).

¹⁶F. M. F. de Groot, M. Grioni, J. C. Fuggle, J. Ghijsen, G. A. Sawatzky, and H. Petersen, *Phys. Rev. B* **40**, 5715 (1989).

¹⁷J. Stohr, K. Baberschke, R. Jaeger, R. Treichler, and S. Brennan, *Phys. Rev. Lett.* **47**, 381 (1981).

¹⁸F. M. F. de Groot, *J. Electron Spectrosc. Relat. Phenom.* **67**, 529 (1994).

¹⁹C. Aruta, G. Ghiringhelli, A. Tebano, N. G. Boggio, N. B. Brookes, P. G. Medaglia, and G. Balestrino, *Phys. Rev. B* **73**, 235121 (2006).

²⁰M. Grioni, M. T. Czyzyk, F. M. F. de Groot, J. C. Fuggle, and B. E. Watts, *Phys. Rev. B* **39**, 4886 (1989).

²¹M. Zangrando, M. Finazzi, G. Paolucci, G. Comelli, B. Diviacco, R. P. Walker, D. Cocco, and F. Parmigiani, *Rev. Sci. Instrum.* **72**, 1313 (2001).

²²M. Zangrando, M. Zacchigna, M. Finazzi, D. Cocco, R. Rochow, and F. Parmigiani, *Rev. Sci. Instrum.* **75**, 31 (2004).

²³P. Reutler, O. Friedt, B. Büchner, M. Braden, and A. Revcolevschi, *J. Cryst. Growth* **249**, 222 (2003).

²⁴J.-H. Park, C. T. Chen, S.-W. Cheong, W. Bao, G. Meigs, V. Chakarian, and Y. U. Idzerda, *Phys. Rev. Lett.* **76**, 4215 (1996).

²⁵K. Horiba, H. Kawanaka, Y. Aiura, T. Saitoh, C. Satoh, Y. Kikuchi, M. Yokoyama, Y. Nishihara, R. Eguchi, Y. Senba, H. Ohashi, Y. Kitajima, and S. Shin, *Phys. Rev. B* **81**, 245127 (2010).

- ²⁶H. Wu, C. F. Chang, O. Schumann, Z. Hu, J. C. Cezar, T. Burnus, N. Hollmann, N. B. Brookes, A. Tanaka, M. Braden, L. H. Tjeng, and D. I. Khomskii, *Phys. Rev. B* **84**, 155126 (2011).
- ²⁷P. Blaha, K. Schwarz, G. K. H. Madsen, D. Kvasnicka, and J. Luitz, WIEN2K (Technische Universität Wien, Austria, 2001).
- ²⁸D. Okuyama, Y. Tokunaga, R. Kumai, Y. Taguchi, T. Arima, and Y. Tokura, *Phys. Rev. B* **80**, 064402 (2009).
- ²⁹F. De Groot and A. Kotani, *Core Level Spectroscopy of Solids* (CRC Press, Boca Raton, FL, 2008).
- ³⁰J. Stohr and H. C. Siegmann, *Magnetism: From Fundamentals to Nanoscale Dynamics*, Springer Series in Solid-State Physics Vol. 152 (Springer, Berlin, 2006).
- ³¹G. Zampieri, M. Abbate, F. Prado, A. Caneiro, and E. Morikawa, *Physica B: Condensed Matter* **320**, 51 (2002).
- ³²O. Toulemonde, F. Millange, F. Studer, B. Raveau, J.-H. Park, and C. T. Chen, *J. Phys.: Condens. Matter* **11**, 109 (1999).
- ³³K. Garg, N. Saini, B. R. Sekhar, R. K. Singhal, B. Doyle, S. Nannarone, F. Bondino, E. Magnano, E. Carleschi, and T. Chatterji, *J. Phys.: Condens. Matter* **20**, 055215 (2008).
- ³⁴R. Mathieu, M. Uchida, Y. Kaneko, J. P. He, X. Z. Yu, R. Kumai, T. Arima, Y. Tomioka, A. Asamitsu, Y. Matsui, and Y. Tokura, *Phys. Rev. B* **74**, 020404 (2006).
- ³⁵M. Abbate, J. C. Fuggle, A. Fujimori, L. H. Tjeng, C. T. Chen, R. Potze, G. A. Sawatzky, H. Eisaki, and S. Uchida, *Phys. Rev. B* **47**, 16124 (1993).
- ³⁶M. Abbate, F. M. F. de Groot, J. C. Fuggle, A. Fujimori, O. Strebel, F. Lopez, M. Domke, G. Kaindl, G. A. Sawatzky, M. Takano, Y. Takeda, H. Eisaki, and S. Uchida, *Phys. Rev. B* **46**, 4511 (1992).
- ³⁷C. Aruta, C. Adamo, A. Galdi, P. Orgiani, V. Bisogni, N. B. Brookes, J. C. Cezar, P. Thakur, C. A. Perroni, G. De Filippis, V. Cataudella, D. G. Schlom, L. Maritato, and G. Ghiringhelli, *Phys. Rev. B* **80**, 140405 (2009).
- ³⁸J. Herrero-Martin, A. Mirone, J. Fernández-Rodríguez, P. Glatzel, J. Garcia, J. Blasco, and J. Geck, *Phys. Rev. B* **82**, 075112 (2010).
- ³⁹F. Bondino, M. Platé, M. Zangrando, M. Zacchigna, D. Cocco, A. Comin, I. Alessandri, L. Malavasi, and F. Parmigiani, *J. Phys. Chem. B* **108**, 4018 (2004).